PHYSICAL REVIEW B **69**, 144402 (2004)

Structure and magnetism of single-phase epitaxial γ'-Fe_4N

J. L. Costa-Krämer,[1] D. M. Borsa,[2,3] J. M. García-Martín,[1] M. S. Martín-González,[1] D. O. Boerma,[3] and F. Briones[1]
[1]*Instituto de Microelectrónica de Madrid, CNM-CSIC, Isaac Newton 8, PTM, 28760 Tres Cantos, Madrid, Spain*
[2]*Nuclear Solid State Physics, Materials Science Centre, University of Groningen, Nijenborgh 4, 9747 AG Groningen, The Netherlands*
[3]*Centro de Micro-Análisis de Materiales (CMAM), Universidad Autónoma de Madrid, Cantoblanco 28049, Madrid, Spain*
(Received 8 July 2003; revised manuscript received 5 January 2004; published 1 April 2004)

Single phase epitaxial pure γ'-Fe_4N films are grown on MgO (001) by molecular beam epitaxy of iron in the presence of nitrogen obtained from a radio frequency atomic source. The epitaxial, single phase nature of the films is revealed by x-ray diffraction and by the local magnetic environment investigated by Mössbauer spectroscopy. The macroscopic magnetic properties of the γ'-Fe_4N films are studied in detail by means of transverse Kerr effect measurements. The hysteresis loops are consistent with the cubic atomic structure, displaying easy [100] magnetization directions. The films are single domain at remanence, and the reversal is dominated by 180° or 90° domain wall nucleation and propagation, depending on the applied field direction. When 90° domain walls are responsible for the magnetization reversal, this proceeds in two stages, and the measured coercive fields vary accordingly. Magnetic domain observations reveal the two distinct reversal —driven by 180° or 90° domain walls— modes displaying large domains, of the order of mm. From magnetometer techniques, the saturation magnetization, $\mu_0 M_s$, is measured to be 1.8 T. A magneto-optical torque technique is used to obtain a value of the anisotropy constant of 2.9×10^4 J/m^3.

DOI: 10.1103/PhysRevB.69.144402 PACS number(s): 75.70.Ak, 75.70.Kw, 75.75.+a, 41.20.Gz

I. INTRODUCTION

During the past decades, iron nitride compounds were extensively investigated due to their excellent magnetic properties, which make them suitable for applications in high density magnetic storage devices.[1] All iron nitrides are metallic conductors and metastable with respect to decomposition in $Fe+N_2$. The decomposition is limited by kinetic barriers. Among the ferromagnetic nitrides, γ'-Fe_4N phase is of special interest. This nitride has a cubic structure, contains 20 at. % N and is stable at temperatures below 400 °C. The saturation magnetization, $\mu_0 M_s$, was reported to be between ~1.8 and 1.9 T.[2–4]

Up to now, polycrystalline thin films of γ'-Fe_4N were grown on (111) Si substrates by ion beam assisted evaporation[5] and reactive sputtering in a NH_3 atmosphere.[2] With N_2 as reactive gas in a dc magnetron sputtering facility, epitaxial γ'-Fe_4N films were grown on (001) Si substrates with a (002) Ag underlayer, as claimed by Brewer *et al.*[6] (concerning purity, crystal quality, roughness or magnetic properties, no details were reported), and on (001) MgO substrates, as reported by Mattson *et al.*[7] and Loloee *et al.*[8] (those works are mainly focused on the properties of Fe_4N/NbN multilayers). Keeping in mind possible applications in current perpendicular-to-plane devices, Nikolaev *et al.* reported on the growth of high quality epitaxial γ'-Fe_4N films by reactive sputtering on (001) $SrTiO_3$ substrates.[9]

Recently, the interest in iron nitrides has been also triggered by the possibility of developing an all-nitride epitaxial magnetic tunnel junction with epitaxial γ'-Fe_4N as magnetic electrodes and epitaxial Cu_3N as insulating barriers.[10] The intermixing at the interface, commonly observed at metal/metal interfaces, may be reduced due to the Fe-N and Cu-N bonding. High quality epitaxial films of γ'-Fe_4N have been grown on (001) MgO substrates by molecular beam epitaxy of iron in the presence of atomic nitrogen.[11,12] In the present paper, we report on and discuss the magnetic properties of such epitaxial γ'-Fe_4N films.

II. EXPERIMENTAL DETAILS

γ'-Fe_4N films were grown by molecular beam epitaxy (MBE) of iron in the presence of atomic nitrogen obtained from a radio frequency (rf) atomic source. The rf atomic source was operated with mixtures of nitrogen and hydrogen in different ratios and different total pressures. Films of different thickness were grown on (001) MgO substrates. Before growth, the MgO substrates were cleaned by annealing at 600 °C in 10^{-6} mbar O_2. The samples were grown with iron enriched to 99% in ^{57}Fe at deposition rates between 0.01 and 0.015 Å/s. During growth, the deposition temperature was 400 °C. For the growth of pure γ'-Fe_4N films, the total pressure in the rf atomic source was 5×10^{-3} mbar (for a mixture of $20\%N_2+80\%H_2$) or 1×10^{-2} mbar (for a mixture of $50\%N_2+50\%H_2$) and the applied rf power was 60 W.

After growth and cooling to room temperature, the films could be capped *in situ* with Cu_3N layers, to prevent oxidation in air. For structural characterization, we performed x-ray diffraction measurements (XRD) using the Cu$K\alpha$ radiation ($\lambda=0.154$ nm) in a standard $\theta-2\theta$ geometry. Additionally, texture measurements were performed in a Philips X'Pert Materials Research Diffractometer system. The measurements were performed both on uncapped and capped films. Grazing incidence x-ray analysis was used to determined the real thicknesses of the films. The single phase nature of the films was investigated by means of Conversion Electron Mössbauer Spectroscopy (CEMS). The surface morphology was studied in air using Atomic Force Microscopy (AFM). No capping layer was present for the samples used in the AFM study.

The longitudinal magnetization process of the γ'-Fe_4N film was measured by the transverse magnetooptic Kerr effect (MOKE). These measurements were performed on capped γ'-Fe_4N films. The light source was a He-Ne laser of 630-nm wavelength and about 10-mW power. The laser light was polarized in the plane of incidence (p polarization) and directed to the film at about 50° incidence. The magnetic field was applied perpendicular to the plane of incidence using a set of Helmholtz coils, which provide a magnetic field of 70 Oe per ampere circulating through the windings. The reflectivity changes were measured with a photodiode using a differential amplifier to subtract the reflectivity signal offset. A resistor in series with the coil provided a voltage proportional to the current circulating through the coil, proportional as well to the magnitude of the field. Both the applied field and the reflectivity signals were monitored in a digital oscilloscope where the hysteresis loops were visualized. In order to increase the signal to noise ratio without loosing bandwidth, a few hundred acquisitions properly triggered were digitally averaged.

The same setup, (transverse MOKE), but exciting the film's magnetic response with rotating magnetic fields, i.e., fields of constant magnitude and constant angular speed, allowed the measurement of the anisotropy axes distribution. The magnetic field direction was monitored with a Hall probe placed at the film location. A simple fit of the measured reflectivity dependency on the applied field angle yielded the value of the anisotropy constant, once the saturation magnetization value had been known. This technique termed as Magneto Optical Torque (MOT),[13] and similar to the conventional torque technique, obtains the distribution of anisotropy axes with a single measurement, and with a simple fit the value of the anisotropy constant is deduced.

The magnetic domain observations were performed illuminating the film with a Xe lamp, placing a polarizer and an analyzer in the longitudinal configuration at almost extinction conditions, and recording the polarization rotations, resolved spatially, in a digital video camera. After finding the optimum conditions, a whole field loop was recorded. In this setup, the coils allow to produce 28 Oe/A, with a maximum field of about 250 Oe. The field frequency for the video acquisition was 10 mHz, producing 100 s of recorded tape per loop. After recording, the tapes were transferred to a PC and edited. In order to gain contrast, simple digital image treatments —subtracting the video frames at selected field values from those at saturation and contrast enhancement— were performed.

III. RESULTS AND DISCUSSION

A. Structural characterization

XRD $\theta-2\theta$ scans measured for all the grown films revealed only the (002) reflections for both the MgO substrate (cubic; $a=4.21$ Å) and the γ'-Fe_4N film (cubic; $a=3.79$ Å). This implied a well-defined orientation of the nitride film with the c axis normal to the substrate.

The epitaxial nature of the films was concluded from x-ray texture measurements, as shown in Fig. 1 for the sample used for magnetic measurements. The grazing incidence x-ray analysis revealed a thickness of 16-nm Cu_3N/36 nm γ'-Fe_4N for this film. In the $\psi-\phi$ pole scan shown in Fig. 1(a), the presence of only four sharp peaks proves the epitaxial nature of the nitride films. Figure 1(b) shows the peak structure in a ϕ scan at constant $\Psi=55.5°$ in more detail. In both scans the 2θ angle was fixed for the (111) reflection of γ'-Fe_4N. This angle also corresponds to the (111) reflection of Cu_3N.

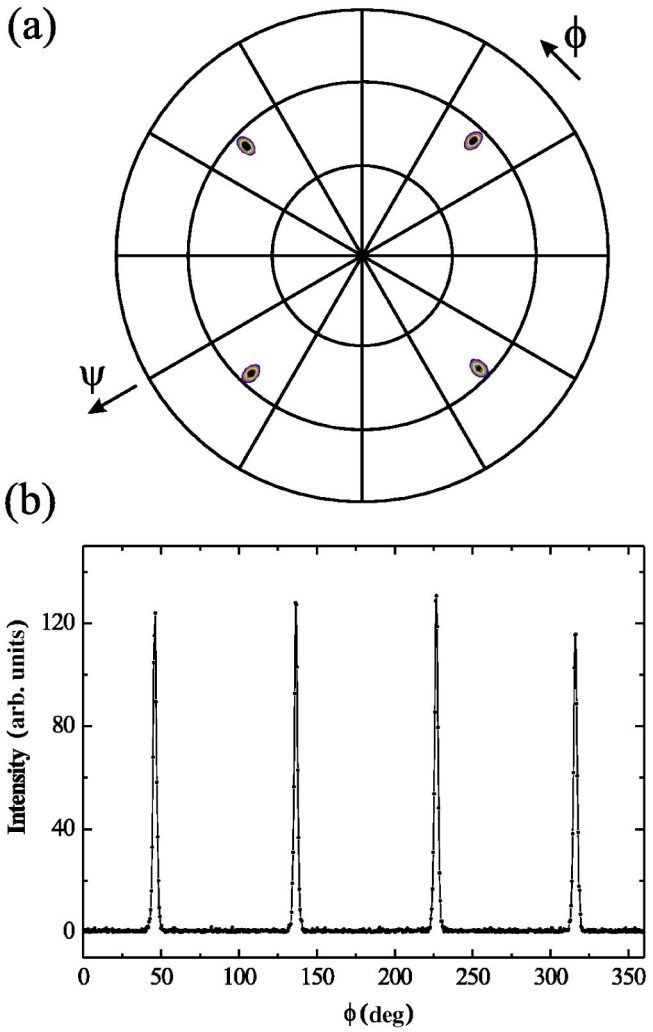

FIG. 1. X-ray diffraction measurements of γ'-Fe_4N films with 2θ fixed for the (111) reflection: (a) $\psi-\phi$ pole scan, and (b) ϕ scan.

The surface morphology of an uncapped film was studied by AFM. Since this sample was uncapped, the top layer could have been transformed into an oxynitride,[12] which can slightly alter the surface structure. Figures 2(a) and 2(b) show AFM images of a 33-nm-thick γ'-Fe_4N film grown on a (001) MgO substrate at 400 °C. The film exhibits a very uniform granular structure, with individual elongated flat islands and an average size $\sim 50\times 200$ nm^2. These islands show weak signs of square symmetry along the [001] directions. The rms roughness of the film, which is only 0.4 nm, corresponds to an average peak-valley height of approximately three atomic spacings (for a cleaned MgO substrate the rms roughness is 0.07 nm). For a 15-nm-thick sample, also deposited at 400 °C, we measured a rms roughness of

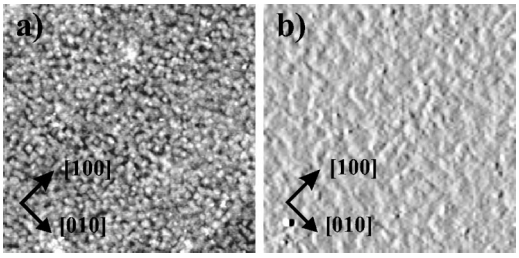

FIG. 2. AFM scans for a 33-nm-thick γ'-Fe_4N film without capping layer. (a) shows the topographical image of a 2.1 $\times$2.1-μm^2 area (vertical range 3.1 nm). (b) shows the force image of a 1.1$\times$1.1-μm^2 area. A smooth, regular surface with weak signs of cubic symmetry was observed.

0.2 nm. The observation of island structure combined with a low roughness points to a layer-by-layer growth process, in which islands are formed, which eventually coalesce in full layers. Additional AFM measurements on samples grown at a lower deposition temperature showed that the roughness decreases with increasing deposition temperature.

B. Magnetic characterization

As firstly discovered in 1930,[14] the γ'-Fe_4N phase is a ferromagnet. It has a cubic structure which contains two non-equivalent crystallographic iron sites: the iron atoms occupying the corner positions (Fe I) and the iron atoms occupying the face-center positions (Fe II), see crystal structure in Fig. 3(a). The ratio of the Fe I:Fe II is 1:3, and, the corresponding magnetic moments of the two sites are $2.98\mu_B$ for Fe I, and $2.01\mu_B$ for Fe II.[15] From the point of view of the atomic structure of Fe-N alloys, the γ'-Fe_4N iron nitride is the simplest structure where Fe-N chains are combined with Fe-Fe chains. This made possible a detailed analysis of the influence of nitrogen on the electronic structure and hyperfine interaction parameters.[16–19]

In our case, the atomic-N assisted MBE grown γ'-Fe_4N thin films have been investigated with CEMS. The ferromagnetic nature of this nitride makes the Mössbauer spectrum rather complicated. The presence of magnetic field leads to a combined magnetic and electric hyperfine interactions. The Hamiltonian of the system is

$$\hat{H} = -(\vec{\mu} \times \vec{H}) + e\sum_{ij} Q_{ij} V_{ij}, \tag{1}$$

where $\vec{\mu}$ is the magnetic moment of the nucleus, $\vec{H}$ is the magnetic field, Q_{ij} is the tensor of the nuclear quadrupole moment and V_{ij} is the tensor of the electric field gradient (EFG). For an internal magnetic field H making an angle θ with the principal axis of the EFG tensor, the energy levels of the excited nuclear state of ^{57}Fe ($I = 3/2$), are given by

$$E = -g\mu_n H m_I + (-1)^{|m_I|+1/2} \times \frac{eQV_{zz}}{4} \times \frac{3\cos^2\theta - 1}{2} \tag{2}$$

where m_I is the magnetic quantum number and V_{zz} is the principal component of the EFG tensor. For the structure of the γ'-Fe_4N phase, the corner iron atoms (Fe I) have a local cubic symmetry and consequently a zero quadrupole splitting. On the other hand, the face-centered iron atoms (Fe II) have an axial symmetry, for which the principal axis of the EFG tensor at the Fe II sites is parallel to the crystal axes, namely the [001] directions. In one unit cell of γ'-Fe_4N, the angle between the principal axis of the EFG tensor and the internal magnetic field is 90° for two of the Fe II sites (the Fe II-A sites), whereas for the third one (the Fe II-B site), the corresponding angle is 0°. Therefore, due to the orientation of the internal magnetic field, crystallographically equivalent sites are magnetically non-equivalent. The quadrupole splitting (S_Q) is defined as:

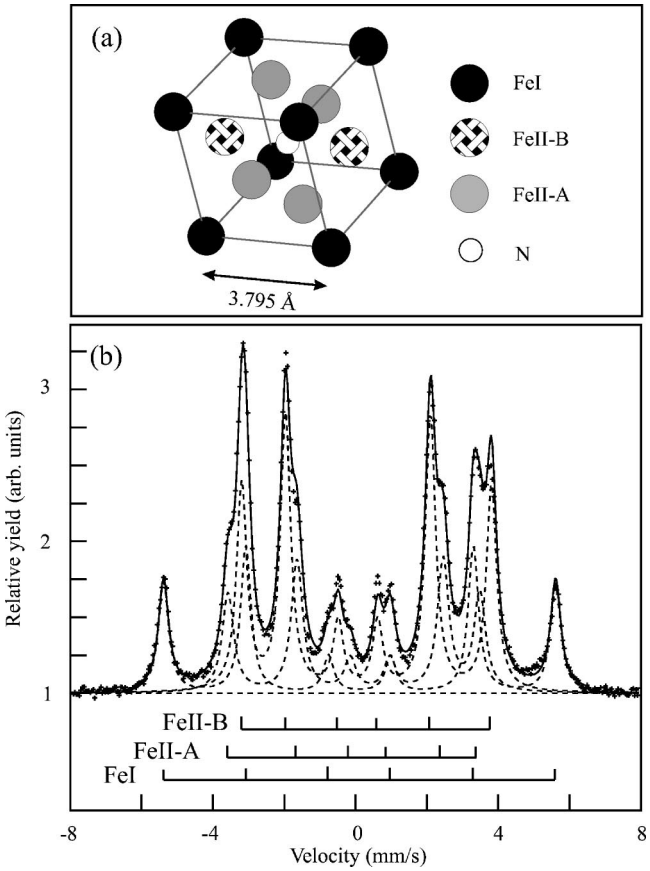

FIG. 3. (a) Crystal structure of γ'-Fe_4N in which the three non-equivalent sites of Fe (Fe I, Fe II-A and Fe II-B) and the N position are shown and (b) room temperature CEMS spectra for a (16-nm Cu_3N)/(36-nm γ'-Fe_4N) sample. The spectrum is fitted with Lorentzian-shaped lines.

$$S_Q = \left(\frac{1}{2}e^2qQ\right)\left(\frac{3\cos^2\theta - 1}{2}\right). \tag{3}$$

From this equation, it is straightforward that the ratio of the quadrupole splitting corresponding to Fe II-A:Fe II-B is 1:-2. All the described features are experimentally confirmed.

The CEMS spectrum measured for a 36-nm-thick γ'-Fe_4N film capped with a 16-nm Cu_3N layer is shown in Fig. 3(b). In this sample only the γ'-Fe_4N layer is Mössbauer active. No external field was applied.

TABLE I. Fit parameters for a γ'-Fe_4N film of 36 nm thickness capped with 16-nm Cu_3N: δ, isomer shift (all given with respect to α-Fe at room temperature); H, hyperfine field; ϵ, quadrupole splitting, R.A., relative area.

Component	δ (mm/s)	H(T)	ϵ (mm/s)	R.A. (%)
Fe I	0.22	34.10	0	25
Fe II-A	0.29	21.72	0.24	50
Fe II-B	0.29	21.89	−0.45	25

The spectrum was de-convoluted in three magnetic components with a 3:4:1:1:4:3 intensity ratio of the lines in each component. The correspondence between the three nonequivalent sites of iron with the deconvoluted peaks has been added at the bottom of Fig. 3(b) for clarification. All the fit parameters are given in Table I. Such a ratio indicates a complete in-plane orientation of the magnetization in the domains. A small (~3%) additional paramagnetic component was used to improve the fit. This component might originate from the γ'-Fe_4N:Cu_3N and γ'-Fe_4N:MgO interfaces. The fit parameters corresponding to γ'-Fe_4N are in good agreement with previous reported data.[20,21]

In Fig. 4 the hysteresis loops measured by transverse MOKE, with the field applied in-plane, and at different angles with respect to the crystalline axes, are shown. The hysteresis loops were measured between 0° and 360° in all the angular range every 5°. Due to the cubic symmetry, loops measured in the first half quadrant, i.e., from 0° to 45°, are representative for all the other quadrants. The vertical axes in all the loops are normalized to the reflectivity changes at magnetic saturation, which is about 1.8% for all the cases. Notice that when the field is applied within a small angular range (35°−45°) around a crystalline [100] axis (45° in Fig. 4), the magnetization switches in a single jump and the reduced remanence, $M_r=(M/M_s)_{H=0}$, is close to one. This happens at a coercive field value of about 80 Oe. This demonstrates that these directions are easy magnetization axes and, as shown later, 180° domain walls drive the reversal. When the field is applied between the easy and hard axes, —loops between 10° and 30°— the reversal takes place in two stages. This is preceded by a reversible rotation of the magnetization, thus reducing the remanence $M_r<1$. The two magnetization leaps point to a reversal process that takes place by two consecutive 90° domain wall nucleation and propagation events, as confirmed later by Kerr microscopy. Finally, when the field is applied close to the hard magnetization axes, the [110] directions (between 0° and 5° in Fig. 4), the loop shows a rotation of the magnetization followed by a sharp reversal and a final rotation. This is consistent with a homogeneous and reversible rotation of the magnetization towards the nearest easy magnetization axis, followed by a 90° driven reversal towards the next easy axis, and a final rotation towards the applied field direction.[22]

The symmetry of the anisotropy becomes more evident when the remanence of the measured loops is plotted versus the applied field angle. This is shown in Fig. 5 in a polar plot, using the values obtained from all the loops measured, including those in Fig. 4. This ''four leaves clover'' plot of the remanence as a function of the applied field is then indicative

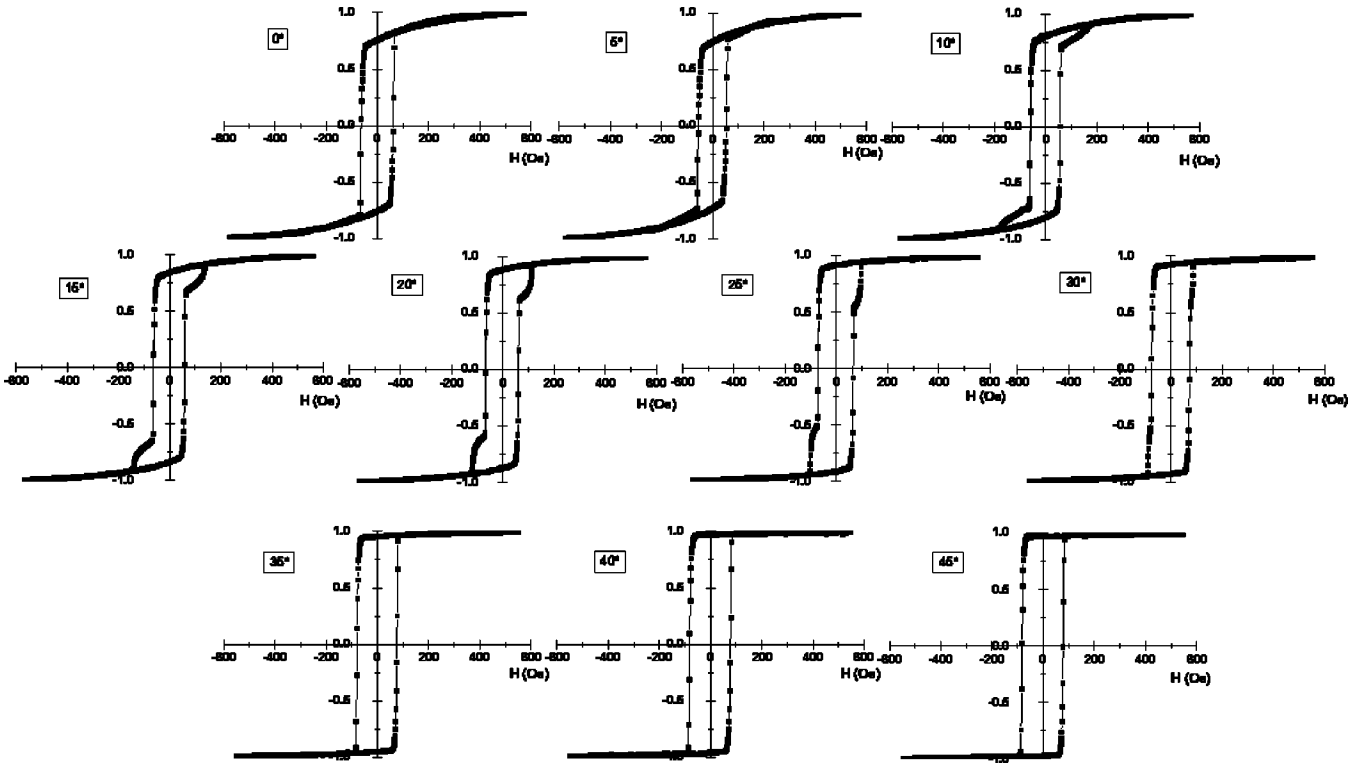

FIG. 4. Epitaxial γ'-Fe_4N film transverse MOKE hysteresis loops with the magnetic field applied along different in-plane directions in the first half quadrant. At 0° the field is applied along the hard [110] magnetization axis

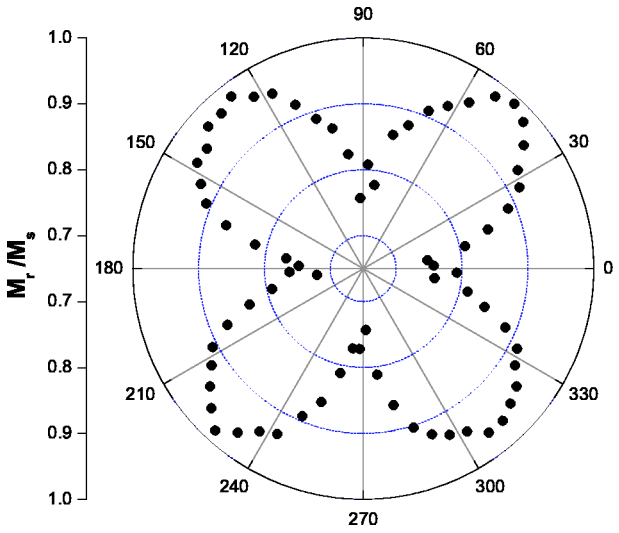

FIG. 5. Reduced remanence M_r as a function of the applied field angle for a γ'-Fe_4N film.

of a biaxial anisotropy due to the crystalline cubic structure of the film. As expected, around the easy magnetization axes the reduced remanence is close to one, and around to the hard magnetization axes the reduced remanence is close to $\cos 45° \simeq 0.71$. The evolution between the hard and easy axes fits a cosine dependence of the applied field angle with the closest easy axis. The values for the reduced remanence points out to a single domain state of the epitaxial film at zero field. The behavior of the sample's magnetization from saturation at maximum field to remanence at zero field can be understood quantitatively with a uniform magnetization and with two relevant energetic contributions, the potential in an applied magnetic field $(\bar{M}\cdot\bar{H})$, and the anisotropy energy determined by the crystal lattice $(K_1/4)\sin^2 2\phi$, where K_1 is the anisotropy constant and ϕ the angle between the magnetization and the nearest easy axis, similarly to the Stoner-Wohlfarth model for a uniaxial anisotropy. Consequently, the minimum energy position is given by the balance of these two contributions, with an equilibrium angle of the magnetization with respect to the field and the crystal lattice axes. Thus, at remanence, the magnetization lays along the crystalline easy axis aligned closest to the applied field direction.

Further evidence of the effect of the anisotropy comes from the reversal mechanism. We have already mentioned that close to the easy axes the reversal takes place by a single process driven by 180° domain wall movement. However, in an angular range of about 25°, between the hard and easy axes, the reversal proceeds in two stages (see Fig. 4), that at first glance, are probably related to two consecutive 90° domain wall movements. The fields at which those sharp events occur are displayed in Fig. 6. For the hysteresis loops with two sharp reversals per half cycle, both values are plotted. As observed in Fig. 6, for the first reversal the coercive field is maximum when the field is applied along the easy axes and minimum when applied along the hard axes. When two switching events occur, the value of the second switching field increases when the field directions becomes closer to a hard axis[23]—see loops between 10° and 30° in Fig. 4. This two transition situation is consistent with a coherent rotation of the magnetization towards the closest easy axis, followed by a 90° domain wall driven transition at the first value of the coercive field to the next easy axis, followed by another 90° domain wall transition to the next easy axis at the second value of the coercive field, and finally a coherent rotation of the magnetization towards the applied field direction. The angular dependence of the coercive fields corresponds to the different projections of the applied field along the easy axes depending on its orientation with respect to them. Finally,

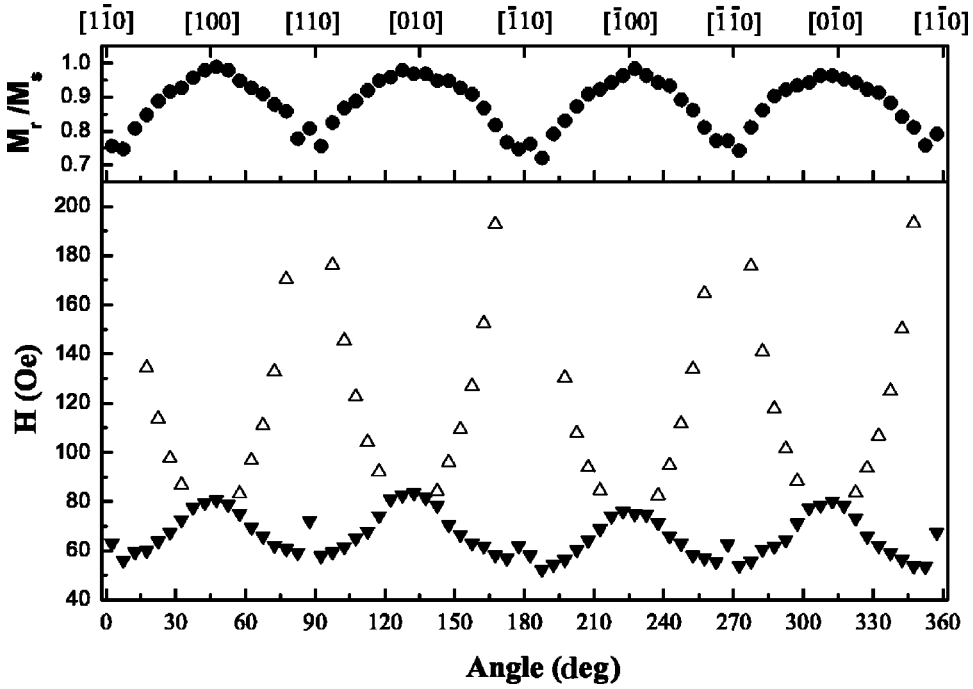

FIG. 6. Bottom: Coercive fields as a function of the applied field angle for the γ'-Fe_4N film. Solid triangles display the field at which the first magnetization switch occurs, while hollow triangles display the field corresponding to the second one when it exists. Top: the same M_r data shown in Fig. 5 in polar plot, for comparison purposes.

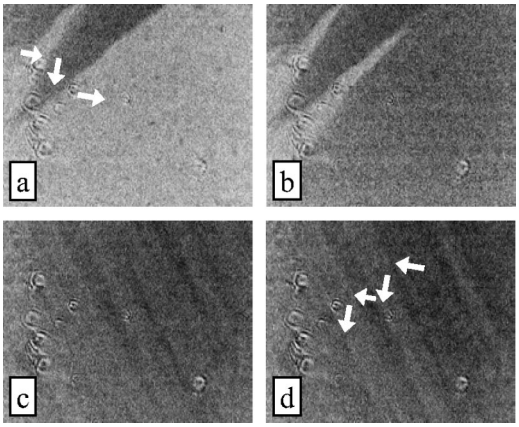

FIG. 7. Kerr domains observations for a epitaxial single phase γ'-Fe_4N film at four consecutive selected field values at an intermediate angle between hard and easy axes (about 15° with respect to the closest easy axis). The images show the domain structure at the first magnetization transition driven by 90° domain walls [pictures (a) and (b)] followed by images at the second transition driven by another set of 90° domain walls [pictures (c) and (d)]. The field is applied horizontally, increasing in magnitude towards the left of the page in this sequence. Field values are (a) 64 Oe, (b) 66 Oe, (c) 84 Oe, and (d) 85 Oe.

when the field is applied within a few degrees from the hard axis, after the rotation towards the closest easy axis, the loops exhibit one single jump, probably due to nucleation and displacement of 90° domain walls. It is important to mention that no evidence of uniaxial anisotropy is present in our measurements, in clear distinction to the behavior reported by Loloee *et al.*[8] where the films exhibited strong uniaxial anisotropy along the (110) direction regardless of their growth either on MgO substrate or on a NbN film.

The main arguments and discussions presented so far are backed by Kerr domain observations at different applied field angles. The sample is rotated with respect to the field in 15° steps, and the camera focused at representative areas and a video sequence acquired. Two representative reversal situations are shown in Figs. 7 and 8. In Fig. 7 the domain structure for a field applied at 15° of the closest easy axis is shown in the same area at four selected field values (a)–(d) corresponding to the two abrupt reversals of the loop. The images span about 490×400 μm^2. Notice, in this case, that the reversal takes place by two subsequent 90° wall propagation events. Figures 7(a) and 7(b) show the domain structure at the first magnetization transition driven by 90° domain walls. Figures 7(c) and 7(d) are two subsequent images at the second transition driven by another set of 90° domain walls. Figures 8(a) and 8(b) show domain images during the reversal, when the field is applied close to one easy axis. The images, about 490×400 μm^2 show adjacent antiparallel domains separated by the 180° domain walls responsible for the reversal in this case.

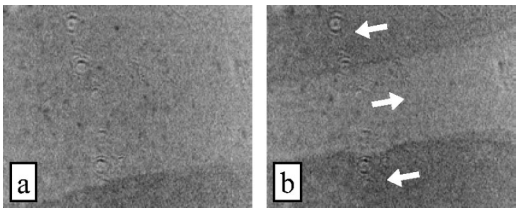

FIG. 8. Kerr domain observations for a epitaxial single phase γ'-Fe_4N film at two consecutive selected field values [78 and 79 Oe for pictures (a) and (b), respectively] along an easy axis. The images show the domain structure at the transition driven by 180° domain walls.

The magnetization properties described so far are consistent with a single phase epitaxial film, having a cubic structure and a positive anisotropy constant, i.e., the [100] directions are easy magnetization axes. All the magnetic characteristics presented so far are then dictated by the value of the anisotropy constant. This value can be estimated from the hysteresis loops obtained applying the field along a hard magnetization axis, if the value of the saturation magnetization is known. In our case, such value have been inferred from magnetic moment measurements of samples whose volumes were estimated by using the thicknesses deduced from grazing incidence x-ray experiments. The room temperature measurements of magnetic moment were performed at 2.5 T in a vibrating sample magnetometer (VSM), and the deduced value of $\mu_0 M_s$ is 1.8 T, similar to those previously reported.[2–4,7–9] It is worth briefly discussing the magnetization evolution with temperature: the γ'-Fe_4N film decomposes at about 400°C into α-Fe and N_2. The VSM measured magnetization decay up to this temperature is just a few percent of the room temperature value, making a Curie temperature estimation based in some kind of extrapolation extremelly inaccurate. In addition, at low temperatures, an anomalous increase of magnetization below 60 K was measured by superconducting quantum interference device magnetometry. As the sample had a capping layer, such an increase can not be attributed to the formation of a ferrihydrite layer on the film's surface, as claimed by Nikolaev *et al.*[9] In summary, the temperature depende of the magnetization needs further investigation and is beyond the scope of the present work.

Once the saturation magnetization was determined, a new magneto-optical method, similar to the conventional torque magnetometry techniques, the so-called magneto-optical torque technique[13] allowed us to obtain the symmetry axes and the value of the anisotropy constant at room temperature with a single measurement and a simple fitting procedure. The method measures the film's magneto optical response in the transverse Kerr configuration to a rotating magnetic field. Whereas conventional MOKE measures the response to a field of constant direction and varying magnitude, in MOT the magnitude of the field is fixed and the field's angle varies. For a sufficiently large field, the sample is magnetically saturated in every direction, and the response corresponds to a homogeneous distribution of the magnetization. This kind of measurement eliminates uncertainties due to domain walls in the anisotropy constant determination.

Figure 9 shows the MOT results for a single phase epitaxial γ'-Fe_4N film at rotating magnetic fields values of (a) 2.3 kG, (b) 1.5 kG, (c) 0.6 kG, and (d) 0.4 kG. The obtained dependencies can be understood as follows. For an infinitely large value of the applied field, the magnetization would be

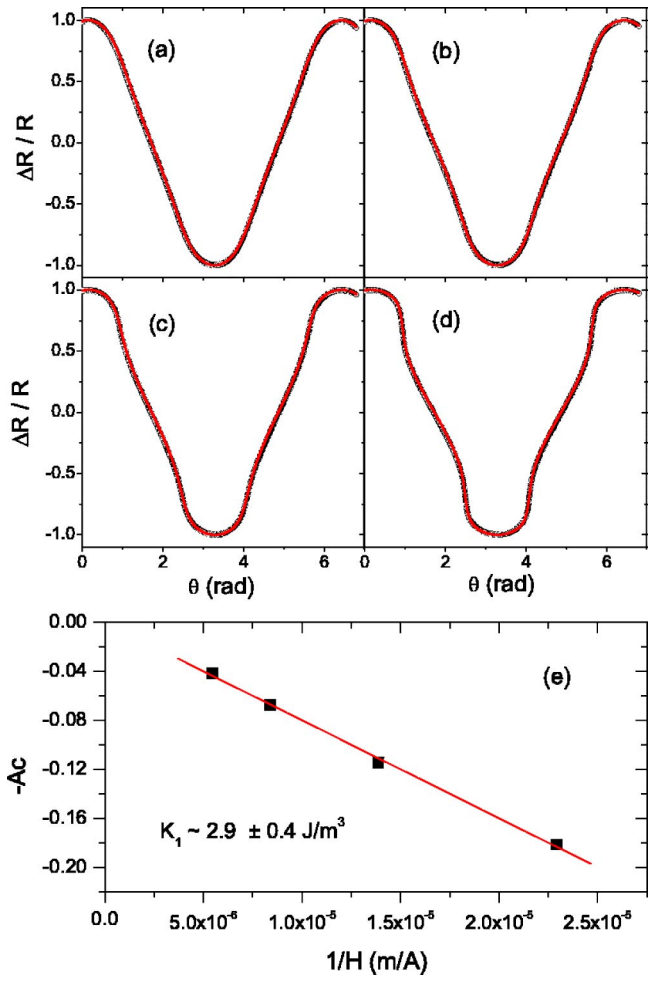

FIG. 9. MOT reflectivity data for a γ'-Fe_4N epitaxial film at rotating magnetic fields of (a) 2.3 kG, (b) 1.5 kG, (c) 0.6 kG, and (d) 0.4 kG. An anisotropy constant of $2.9\pm0.4\times10^4$ J/m^3 ($\times10^5$ erg/cm^3) is obtained

parallel to the field at all angles and the response would be perfectly sinusoidal. The departure from this behavior is due to the anisotropy. For a finite value of the field, when the field direction departs from an easy axis the magnetization lags behind the field, while when the field departs from a hard axis the magnetization leads ahead. The deviations from a sinusoidal dependence are then indicative of the effect of the anisotropy, being more apparent at the crossing of the field through a hard axis. In the graphs, the points represent the obtained data values and the line, overlapping the points, is a fit to the data. The fit only considers the potential energy due to the angle of the applied magnetic field and the saturation magnetization ($\bar{M}\cdot\bar{H}$) and a cubic anisotropy $(K_1/4)\sin^2 2\phi$. The fit depends on only one parameter: $A_c=(K_1/2MH)$. The values of the obtained parameter A_c vs $(1/H)$ are shown in (e) with a linear fit to the data. Taking into account the measured value of the saturation magnetization of γ'-Fe_4N, an anisotropy constant of 2.9×10^4 J/m^3 ($\times10^5$ erg/cm^3) is obtained. It is worth comparing such value to that reported for γ'-Fe_4N prepared by reactive sputtering on $SrTiO_3$ substrates, 1.6×10^4 J/m^3[39]. The anisotropy constant in our films is closer to that of pure bcc iron (4.8×10^4 J/m^3), which can be an indication of higher crystalline quality.

IV. CONCLUSIONS

In summary, the structural and magnetic properties of epitaxial γ'-Fe_4N iron nitrides films have been investigated. The thin films have been grown by MBE of iron in the presence of nitrogen obtained from a rf atomic source. The epitaxial, single phase nature of the films is concluded from x-ray diffraction and Mössbauer spectroscopy measurements. The magnetization reversal processes of pure epitaxial γ'-Fe_4N films have been studied in detail by Kerr measurements. The hysteresis loops are consistent with a cubic symmetry, displaying easy [100] magnetization directions. The film is single domain at remanence, and the reversal is dominated by 180° or 90° domain wall propagation, depending on the applied field direction. When 90° domain walls are responsible of the magnetization reversal, this proceeds in two stages, and the measured coercive fields vary accordingly. Magnetic domain observations corroborate these conclusions, obtaining large domains during the reversal of the order of mm. From room temperature measurements of magnetic moment, the saturation magnetization is deduced, $\mu_0 M_s$ being 1.8 T. Finally, a magneto-optical torque technique is used to obtain a value of the anisotropy constant of 2.9×10^4 J/m^3.

ACKNOWLEDGMENTS

The authors acknowledge partial financing from EC project HIDEMAR G5RD-CT-2002-00731 and PHANTOMS network. The authors are indebted to A. Gupta and K. V. Rao from the department of Materials Science and Engineering, KTH, Sweden for help with the low T SQUID measurements, and to L. Ballcels and M. A. García from Materials Science ICMM CSIC, Spain for high-*T* VSM measurements. This work was part of the research program of the Foundation for Fundamental Research on Matter-FOM, The Netherlands. J.M.G.M. acknowledges financing through the Ramón y Cajal program from the Spanish MCyT.

[1] J. M. D. Coey and P. A. I. Smith, J. Magn. Magn. Mater. **200**, 405 (1999).
[2] J. Q. Xiao and C. L. Chien, Appl. Phys. Lett. **64**, 384 (1994).
[3] T. Takahashi, N. Takahashi, N. Tamura, T. Nakamura, M. Yosioka, W. Inami, and Y. Kawata, J. Mater. Chem. **11**, 3154 (2001).
[4] T. Yamaguchi, M. Sakita, M. Nakamura, and T. Kobira, J. Magn. Magn. Mater. **215**, 529 (2000).
[5] H. Chatbi, M. Vergnat, Ph. Bauer, and G. Marchal, Appl. Phys. Lett. **67**, 430 (1995).

[6] M. A. Brewer, K. M. Krishnan, and C. Ortiz, J. Appl. Phys. **79**, 5321 (1996).
[7] J. E. Mattson, C. D. Potter, M. J. Conover, C. H. Sowers, and S. D. Bader, Phys. Rev. B **55**, 70 (1997).
[8] R. Loloee, K. R. Nikolaev, and W. P. Pratt, Appl. Phys. Lett. **82**, 3281 (2003).
[9] K. R. Nikolaev, I. N. Krivorotov, E. D. Dahlberg, V. A. Vas'ko, S. Urazhdin, R. Loloee, and W. P. Pratt, Appl. Phys. Lett. **82**, 4534 (2003).
[10] D. M. Borsa, S. Grachev, C. Presura, and D. O. Boerma, Appl. Phys. Lett. **80**, 1823 (2002).
[11] S. Grachev, D. M. Borsa, S. Vongtragool, and D. O. Boerma, Surf. Sci. **482–485**, 802 (2001).
[12] D. M. Borsa, S. Grachev, D. O. Boerma, and J. W. J. Kerssemakers, Appl. Phys. Lett. **79**, 994 (2001).
[13] G. Armelles, J. L. Costa-Krämer, J. I. Martín, J. V. Anguita, and J. L. Vicent, Appl. Phys. Lett. **77**, 2039 (2000).
[14] E. Lehrer, Z. Elektrochemie **36**, 382 (1930).
[15] B. C. Frazer, Phys. Rev. **112**, 751 (1958).
[16] W. Zhou, L. J. Qu, Q. M. Zhang, and D. S. Wang, Phys. Rev. B **40**, 6393 (1989).
[17] Y. Kong, J. Pelzl, and F. Li, J. Magn. Magn. Mater. **195**, 483 (1999).
[18] A. N. Timoshevskii, V. A. Timoshevskii, B. Z. Yanchitsky, and V. A. Yavna, Comput. Mater. Sci. **22**, 99 (2001).
[19] P. Mohn and S. F. Matar, J. Magn. Magn. Mater. **191**, 234 (1999).
[20] J. C. Wood, Jr. and A. J. Nozik, Phys. Rev. B **4**, 2224 (1971).
[21] C. A. Kuhnen, R. S. de Figueiredo, V. Drago, and E. Z. da Silva, J. Magn. Magn. Mater. **111**, 95 (1992).
[22] E. Gu, J. A. C. Bland, C. Daboo, M. Gester, L. M. Brown, R. Ploessl, and J. N. Chapman, Phys. Rev. B **51**, 3596 (1995).
[23] R. P. Cowburn, S. J. Gray, J. Ferré, J. A. C. Bland, and J. Miltat, J. Appl. Phys. **78**, 7210 (1995).